Recent Advancements in Additive Manufacturing (AM) Techniques: A Forward-Looking Review

Netrapal Singh[1,2] · Hafsa Siddiqui[2] · Bhavani Srinivas Rao Koyalada[2] · Ajay Mandal[1,2] · Viplov Chauhan[3] · Sathish Natarajan[1,2] · Satendra Kumar[1,2] · Manoj Goswami[1,2] · Surender Kumar[1,2]

Abstract

We witness noteworthy developments in multifunctional materials progress through additive manufacturing techniques, enhanced by the revolution of Industry 4.0 and Internet of Things. Still, in specific circumstances, the performance of used materials is sometimes limited. Among the various existing techniques, the additive manufacturing (AM) process has gained much popularity over the last two decades and is one of the most revolutionary manufacturing techniques. In this comprehensive review, we have addressed the fundamentals of various Additive Manufacturing processes, including binder jetting, fused deposition modelling, Stereolithography, selective laser sintering/melting, direct energy deposition. Furthermore, recent advancements and emerging new technology in AM domain named electrochemical additive manufacturing is highlighted in this review as a major part. These processes' capabilities, advantages, limitations, and applications are also discussed. In the concluding sections of this work, future trends are offered and discussed.

Keywords BJT · FDM · SLA · SLS · SLM · ECAM

1 Introduction

1.1 AM processes

Fabricating any physical object, manufacturing processes always play a crucial role in human life. The existence of manufacturing techniques in our life is from ancient times when our ancestors used stones to prepare several tools. Various manufacturing methods exist, such as casting, moulding, machining, forming, joining, AM, etc. Among the different existing techniques, the AM process has gained much popularity over the last two decades and is one of the most

Netrapal Singh and Hafsa Siddiqui have been contributed equally to this work.

✉ Surender Kumar
  surenderjanagal@gmail.com; surender@ampri.res.in

[1] Academy of Scientific and Innovative Research (AcSIR), Ghaziabad 201002, India

[2] CSIR-Advanced Materials and Processes Research Institute (AMPRI), Bhopal 462026, India

[3] Department of Physics, Institute for Excellence in Higher Education, Bhopal 462016, India

revolutionary manufacturing techniques. AM, as the name implies, adds requisite material in layer upon layer fashion to obtain a final three-dimensional (3D) product. Rapid prototyping, 3D printing, additive layer manufacturing, additive fabrication, layer manufacturing, additive processes, and freeform fabrication are other names that AM is known in the scientific community [1].

In the AM process, we transform a computerized 3D solid model (computer-aided design- CAD) into a finalized product with satisfactory geometric accuracy without using additional fixtures or cutting tools, like the conventional subtracting manufacturing processes [2, 3], though sometimes there is a need of post-processing. Thus, in that sense, AM has a better ability to handle the raw materials, as there are fewer chances of waste, and it opens up the possibility of forming more complex geometrical components [3]. Figure 1 shows the steps involved in the AM process to transform the element from the digital world to the real world. The AM process broadly applies to various materials such as ceramics, metals, polymers, composites, etc. [1]. Multiple AM approaches are available these days for processing this wide variety of material; some of these techniques are SLM, SLS, DED, and FDM [4]. The working principle applied in these techniques varies from type

Fig. 1 Schematic representation
of AM Process
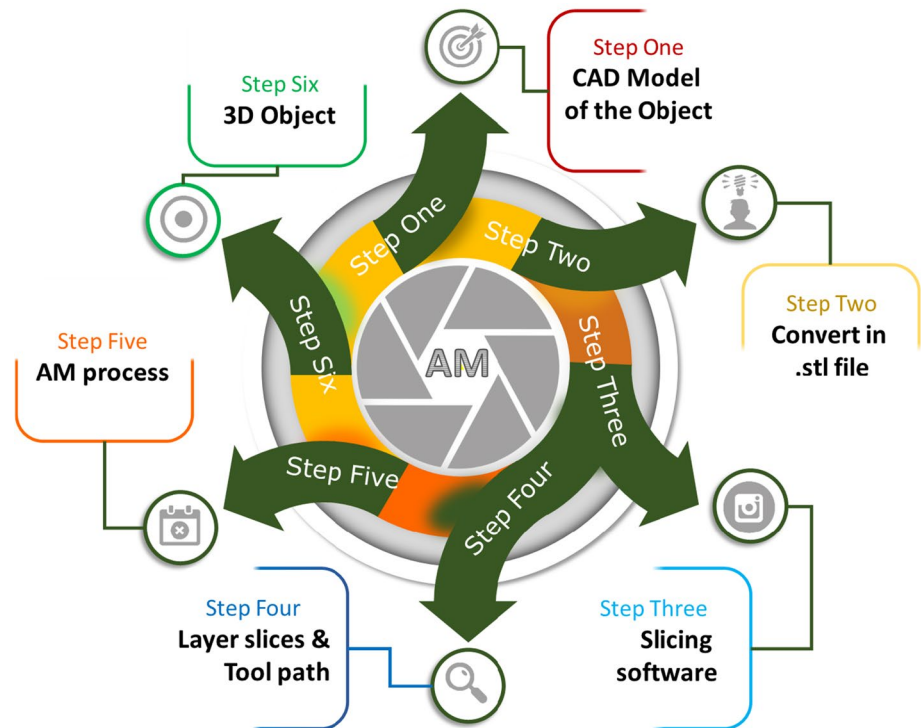
to type. In SLM and SLS, the metal powder is melted or sintered selectively using a high-power laser [5]; on the other side, in FDM, the polymer is fed as a filament, which is extruded from heated nozzle followed by deposition [6].

For metallic materials recently, Wire Arc AM (WAAM) is also gained colossal attention; the WAAM process is very much similar to the polymer-based FDM technique, where polymer wire is extruded from a heated nozzle. Apart from the heated extruder, in WAAM, the metallic wire is melted using a laser beam that is highly directed [7]. However, an in-depth discussion of these methods is beyond the scope of this review. Regarding polymer AM, some other techniques are vat photopolymerization. In vat photopolymerization, we use a light-sensitive polymer liquid or resin [8]. SLA is one of the commonly used vat photopolymerization methods, in which a coherent beam of light (generally of the ultra-violet spectrum) is used for photopolymerization. Due to this, the resin becomes solidified in layer by layer manner for fabrication of the end product [8]. Material jetting, BJT, continuous liquid interface production, digital light processing, laminated object manufacturing, two-photon and multiphoton polymerization, drop-on-demand process, DED [9], and inkjet printing [10] are other various commercially available AM techniques. Besides, ECAM is a very recent form of the metal AM process. Here, we can create metallic structures using the electrodeposition phenomenon in a localized manner. The key benefit of the process lies in its applicability to an extensive range of materials and

alloy deposition ambient conditions [11]. All the above-discussed techniques have pros and cons [12] and are discussed in detail in Sect. 2.

1.2 About the Review

This review aims to initiate AM research and gather information on the working modes of different commercially used AM technologies. Current overview of BJT, FDM, SLA, SLS, SLM and ECAM processes, including structure-property relationships, dimensional control and engineering, interfaces and some theoretical and modelling studies along with future scope are presented. A key interesting aspect of AM processes is the recognition of the realities of inter-disciplinary research between various fields of mechanical engineering (power-generating machines) as well as physics, chemistry, industrial, and commercial applications such as automotive and aerospace industry, medical industry, construction and the jewellery industry.

2 Recent Advancements in AM Techniques

A brief introduction to various AM techniques is given in Sect. 1. This section aims to provide a detailed insight into selected AM methods, including BJT, FDM, SLA, SLS, SLM, and ECAM processes.

2.1 Binder Jetting (BJT)

BJT is an AM technique invented at the Massachusetts Institute of Technology (MIT), United States of America (USA), in 1993. It was developed very early in AM process evolution [13]. BJT is used for making sand moulds for casting and metal and ceramic components. BJT is depicted schematically in Fig. 2. The procedure begins with a powder re-coater system, which typically consists of rollers, spreading a thin layer of required powder. After that, a liquid ink, called the binder, is selectively jetted using an inkjet nozzle, according to a 3D CAD model of the desired component. The binder is then evaporated using a lamp-based heater, releasing the stacked particles behind [14, 15]. Heaters may be used in some systems for moisture-controlling and curing purposes, but it is still not mandatory. After completion of the first layer, the building platform lowers by a distance equivalent to the height of the sliced layer, and this procedure is repeated until the three-dimensional part is built. Thus, an obtained body, called the green body, is immersed in unbound powder and needs sequential post-processing steps to improve its mechanical properties and a finalized usable product [15]. Since the material to be printed is fed in the form of powder, then choosing the suitable powder is very important. Flowability, bulk density, morphology, size and distribution of particles are vital factors that should be considered when selecting a material powder. Otherwise, they will primarily affect the final properties of the component [16]. Flowability, in some sense, predicts printability as we need to spread the powder uniformly over the bed, which directly relates to flowability.
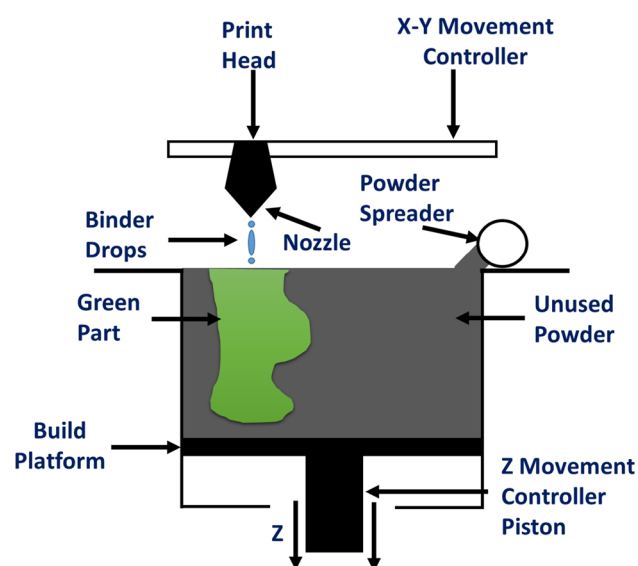

Fig. 2 A schematic of a typical binder jetting 3D printing process

If we have a powder with poor flowability, it would not be spread evenly and smoothly and hence, cause defects in the printed 3D object. Fortunately, it is easy to control the flowability of the powder using spray granulation and additives [16–18]. Flowability of the powder also shows a high dependence on shape of the powdered particles. Particles having a spherical shape tends to flow more than others. The size of the particles also plays a key role; for example, the system will experience issues if the powder particle size is greater than the thickness of the sliced layer. Generally, powders of particle size between 0.2 and 200 μm are used [19, 20]. Finer particles (with a size < 20 μm) do not possess good flowability, while the coarser one (with a size > 20 μm) flows better [21–23]. Binder is the material that binds the powder particles of the material to be printed; thus, the selection of a suitable binder is essential. The binder should be low viscous, stable against the stresses generated during the printing process, economical, environment friendly, and should not block the nozzle. Besides, a binder must interact well with the powder particles [15, 24]. After selecting a suitable powder and binder, one must form an ink for printing. The formulation process includes engineering according to the print head's viscosity and surface tension checking its stability and redispersion behaviour, and reformulation if needed [21]. After the formulation of ink, the printing process is initiated. The density, fineness, and strength of the printed object [16] are all affected by the layer thickness, which is measured as the elevation of a layer along the z-direction, the speed at which powder is dispersed onto the printing bed, the printing speed, binder concentration, and printing direction [25–30].

Printed binder jetting products are generally not up to the mark in terms of their mechanical strength and need further treatment to strengthen them and make them ready for the final application. The green body is a sinter to densify the product, providing the required mechanical strength [31, 32]. The appropriate time and temperature selection for sintering are significant to ensure proper sintering and diffusion between particles. Depowdering is another post-process that the green body undergoes. In depowering, the extra powder around the green body is removed [16]. Therefore, the depowdering process should be carried out carefully to avoid the printed parts' breakage.

The precise printing nature of the BJT has opened a new revolution in medicine and pharmaceutical. The printing of biomaterials as scaffolds in bone tissue engineering, fabrication of ceramic materials for dental applications, the printing of implants and various tools for medical applications and manufacturing of pharmaceutical dosage is very commonly used applications of BJT [33, 34]. Also, BJT is among the few AM processes used for food 3D printing. Researchers have 3D printed the sugar and starch mixtures using BJT [35]. Moreover, the ability of BJT to print multi-materials,

electrically conductive devices, and construction industry materials such as cement, mortar, sand, gypsum etc., sets it apart from other AM techniques and indicates its broad-ranged applicability [36, 37].

Though the BJT offers applications in a broad spectrum of fields, some significant issues still need rectification. The selection of proper-sized powder particles, binder and optimum printing parameters is substantial. The agglomeration of small-sized powder particles also creates printing defects. Moreover, post-processing is the biggest concern with BJT. Since the as-printed 3D objects are not up to the mark, they require proper infiltration and heat treatment to get the desired mechanical strength. This makes the printing process very slow and increases the net cost of the printed parts [37].

2.2 Fused Deposition Modelling (FDM)

Stratasys Inc., a United States based company, was the first to invent an FDM 3D printer. It is one of the most popular, commonly used and rapidly expanding AM processes [38]. Thin wire of thermoplastics is utilized as the raw material in FDM and is extruded from a heated nozzle. The motion of the nozzle is guided by the combination of stepper motors; the movement of the nozzle is according to the Gcode as per the 3D CAD model of desired component. FDM is generally used for thermoplastic polymeric material only, like acrylonitrile butadiene styrene (ABS), polycarbonate (PC), polylactic acid (PLA), Nylon, polyphenyl sulfone (PPSF), PC-ISO, PC-ABS blends etc. [39]. However, after continuous scientific input and advancement in this technology,e fascinating materials such as carbon, glass and Kevlar fibre composite [40, 41] and metal powder-reinforced polymer composite [42] can also be printed by the FDM process. The mechanical properties of these composites are comparable to several metallic materials [43]. Therefore, FDM technology is widely used to fabricate parts with applications in electronics, mechanical systems, aerospace, and the automobile industry. Otherwise, FDM was primarily used for prototyping purposes only [38].

In FDM, the extrusion nozzle is heated to soften or melt the material. The temperature of the nozzle depends upon the material to be deposited. For example, the nozzle temperature is generally kept at 240–250 °C and 190–200 °C for ABS and PLA, respectively. The extruded material solidifies and takes the desired shape by cooling as the build platform's temperature is shallow compared to the nozzle (~ 70 °C for PLA). When the very first layer of the polymer material is deposited, the build surface moves in a vertical direction, a height equals the thickness of the layer [38, 39]. The thickness of a single deposited layer may vary from 0.06 to 0.4 mm, depending on the system and settings used. The vertical motion is of two types: the build platform moves downward, or the extruder moves upward, depending upon the machine being used. The subsequent material layer is added at top of the preceding layer, and process is repeated until the desired final structure is achieved. Sometimes, support structures are needed for complex geometries or hanging parts [38, 44]. A diagram of the FDM machine is shown in Fig. 3.

The final printed product's quality depends on a variety of factors, like the solidification process of the polymer used, the thermal gradients between the print head and build chamber, the crystallization process of polymers, the viscoelastic properties of the material, shrinkage effect, and generation of residual stress during the printing process [45–48]. These days, we can now produce real-time usable products [48]. Biomedical [49, 50], electronics [51], tooling and machining [52], and aerospace [53] are some of the areas which are using FDM for various purposes. The key benefits of this technique lie in the availability of a wide range of feedstock materials [54]. This provides additional flexibility to the users [55].

Despite being among the most widely used and useful AM processes, FDM still has some serious challenges. Surface roughness, the need for the support structure, the requirement of post-processing, low resolution, low printing speed, low dimensional accuracy, generation of residual stresses because of the temperature gradient between the build platform and the print head, lack of high-quality
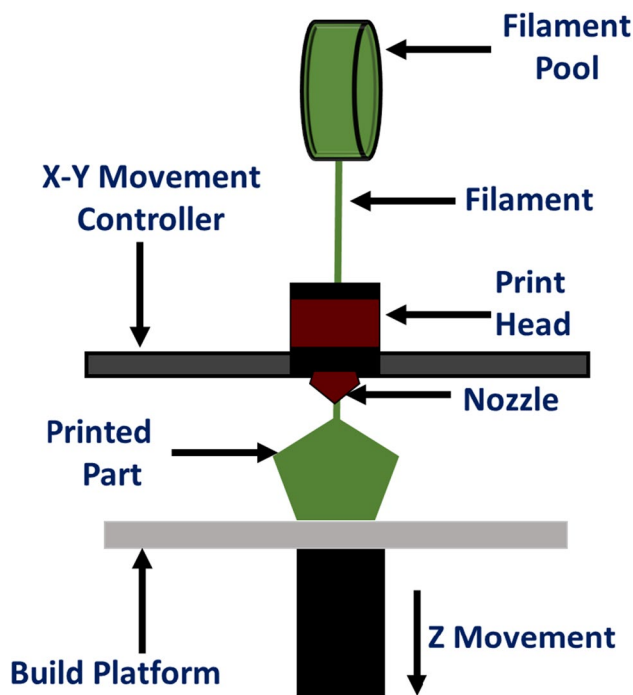

Fig. 3 Schematic diagram of a typical FDM-based 3D printer

finishing, etc. are some the major challenges related to the fused deposition modelling [54, 56–58].

2.3 Stereolithography (SLA)

This is a resin-based polymer AM technique, in which raw material is used in form of resin. This technology works on the principle of the photopolymerization technique. In this process, photo polymeric polymer resin is used as a raw material, solidifying gradually in a layer-by-layer manner on light exposure with a specific wavelength. An ultra-violet (UV) light source is typically used [59, 60]. It takes only a few milliseconds to a few seconds (depending on the quality of the resin) to solidify the resin. UV light source is allowed to move in accordance with the given CAD model; after the layer has fully hardened, the build platform is moved lowered by the thickness of a single layer, after which fresh resin contacts the layer that has already solidified and is then scanned by a UV light source [61, 62]. This step will be repeated again and again until the entire geometry is completed [59, 61]. Figure 4 represents the schematic of the SLA system. Finally, the printed object is removed from the build surface and cured in the chamber for a specific time to strengthen it. SLA process spans a broad spectrum of fields, including industry and engineering, soft robotics, smart composites, flexible electronics, medical and biomedical, superhydrophobic 3D objects, prosthetics and orthotics, jewellery, sports equipment, etc. Recent studies have projected the massive potential of the SLA process in nano 3D printing and 4D printing [8].

Post-processing is the major area where the SLA process lacks. Various materials, particle sizes, or solid loadings introduce diversity during post-processing, ranging from the delicacy of green parts during support removal to the ultimate shrinkage, porosity, and deformities of the sintered component. Green parts are base polymerized parts obtained
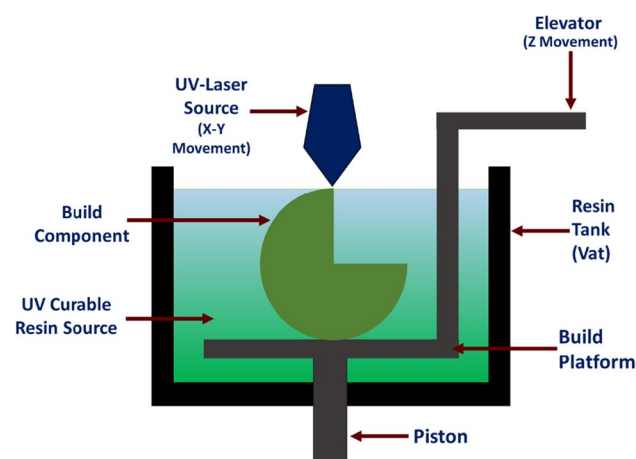

Fig. 4 Schematic illustration of stereolithography 3D printing

through SLA 3D printing. They are the solid suspension of the desired material and polymer in the polymer matrix. The delicate nature of the green parts further leads to the complication of removing the printed objects from the build platform. Properly optimizing the positioning of parts and support structures on the build platform can ease this process. Removing the support structures can also cause damage to the final product and hence are to be taken care of properly. Moreover, some printed objects may also require sintering to obtain the desired mechanical strength [63].

2.4 Selective Laser Melting (SLM)

The SLM process is helpful for metals only. Here, the raw material is used in as the power particles. This technique is among the most widely used AM technologies in manufacturing industries for the fabrication of highly efficient, lightweight and complexly designed end-user components to be used in automobile, aerospace as well as defence sectors [64, 65]. Figure 5 depicts the basic principle of the SLM process: a very thin layer of metal powder is first placed on the building surface through a powder recorder setup. Then, in a confined space, a powerful laser is used to melt this thin metal powder layer as per the provided CAD model of the desired component [66, 67].

Before melting, the substrate (build platform) is also heated at a specific temperature (depending on the type of material used) to minimize thermal stresses in the final component and avoid peeling off the component. Also, everything is placed inside the closed chamber filled with high-purity argon, so that oxidation of metal powder during melting can be prevented. A small molten pool was formed, which solidified rapidly with a solidification rate of 10^6 to 10^8 K/s [67, 68]. The laser restarts the melting process once a layer is completely melted; a subsequent layer of the fresh powder is dispersed over the recently deposited layer utilizing the recording system. The process is continued until the last complete component is built. The part is then left for the cool-down process, typically needed to lower the temperature of the whole component so that it can be handled easily and exposed to the open environment. Finally, the part is removed from the build chamber, loose powder is appropriately cleaned, and secondary operations are performed if necessary [64, 67].

Although significant achievements have been made in understanding the SLM technique and manufacturing a wide range of materials utilizing this technology, commercial uses are still minimal. Some of the critical obstacles hidden in this approach that prohibit it from creating functioning components are limitations associated with printing multimaterials, insufficient expertise on the optimal processing parameters for innovative materials, and high porosity on the parts produced [69]. To overcome these issues and to

Fig. 5 Schematic representation of the selective laser melting (SLM) process
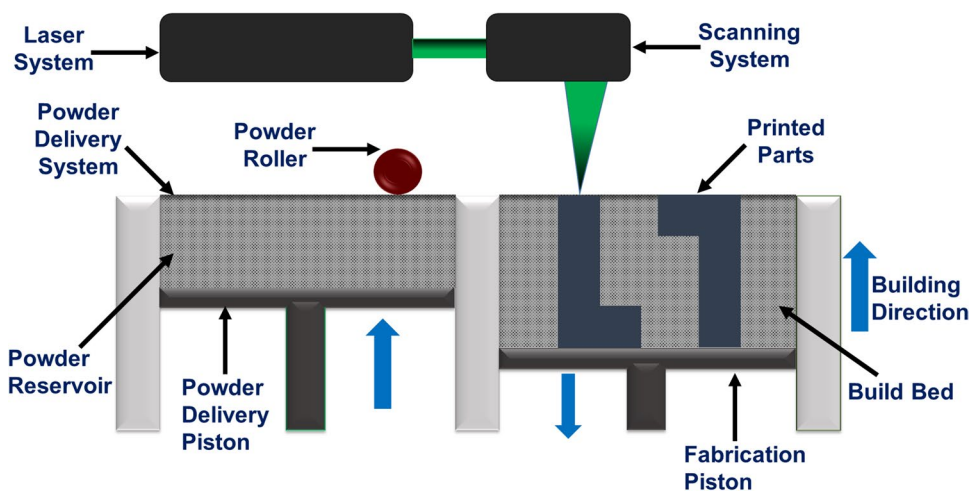
determine the ideal operating conditions for the SLM technique, the most critical SLM process factors, such as laser power, scan speed and strategy, layer thickness, and build orientation, should be thoroughly explored [70]. Any form of imperfection, such as porosity, surface texturing, dimensional inaccuracy, and so on, may occur during the printing of the objects. That's why proper post-processing methods such as thermal treatment, ageing, solution treatment, chemical treatments, and other approaches should be utilized in reducing problems associated with the printing process. Moreover, removing the support from as-printed material is a complicated process since it may damage the printed objects; hence, the minimum support structures should be used [71].

2.5 Selective Laser Sintering (SLS)

The basic principle and setup used in SLS are the same as SLM; the only difference in both is the phenomena of powder particle binding. Unlike SLM, SLS powder particles get sintered together rather than completely melting. Sintering is used in powder metallurgy to describe the powder particles' fusion (in solid-state) when exposed to an elevated temperature below the material's melting point[72–75]. According to the literature, minimizing powder particles' surface energy (ES) is the driving factor for solid-state sintering. E_S is proportional to the surface area of a total particle (S_A), as shown in the equation below:

$$E_S = \gamma_s \times S_A$$

where γs is surface energy per unit area for a particular atmosphere, material, and temperature. In SLS, when powder particles fuse under the exposure of laser beams, surface area decreases which finally reduces the surface energy [76]. Because smaller particles' higher surface area to volume ratio experiences a larger driving force for necking and

consolidation, smaller particles get sintered more quickly and at much lower temperatures than larger particles[77, 78]. This concept emphasizes researchers' use of finer powder in SLS. Figure 6 shows the steps involve in the sintering process. When working with SLM and SLS, it's essential to be cautious when choosing the required process parameters, which includs laser scanning speed and power, layer thickness, and hatch spacing. However, these processes consist of numerous parameters that must be controlled and observed carefully before starting the machine. Out of all the other parameters, the mentioned parameters are the most important ones, as their combination decides the laser energy density (Q) value (as shown in the equation below). The final properties of the build component depend on the value of Q, and the selection of the process parameters depends on the type of material needed. The choice of inappropriate process parameters will lead to formation of unwanted defects like pores, keyholes, cracks etc. The detailed discussion regarding the defects is out of the scope of the present article.

$$Q = \frac{Laser\ power}{Hatch\ spacing \times Layer\ thickness \times Scanning\ Speed}$$

SLS has many benefits in comparison with other AM technologies, like lack of support structures and superior mechanical qualities similar to injection moulded products. However, numerous shortcomings, such as the highly porous printed parts and limited availability of SLS powder particles, continue to limit its capability to deal with materials [79].

2.6 Direct Energy Deposition (DED)

The DED process has been very commonly used in laser-based manufacturing industries for a long time. This process is not a 3D printing process, but its working principle is
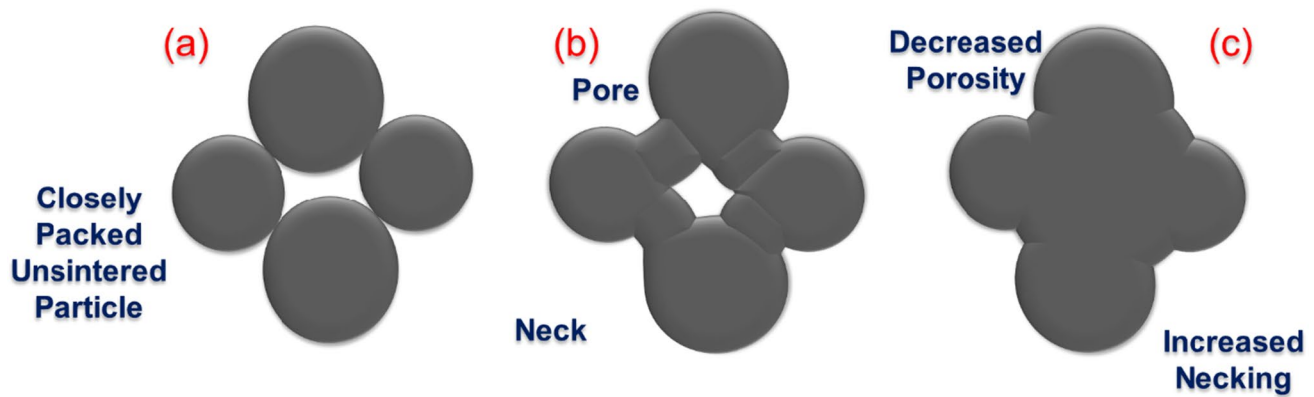
Fig. 6 Sintering process **a** Closely packed powder particles before sintering, **b** Necking phenomena occur with the increase in temperature, particles start diffusing into each other due to which its surface area decrease and free energy minimize, **c** Pore size decreases with time

the same, i.e., layer-by-layer material deposition. Presently, industries use this process to manufacture new components; previously, it was used for repairing and joining damaged components only. It is not a powder bed process like SLM and SLS; here, the powder form feed from the nozzle on the build area, where it is get melted with the help of a focused laser beam. The feedstock nozzle and laser source are mounted on a motorised robotic arm, which moves according to 3D CAD geometry and simultaneously gets deposited layer-by-layer. Everything is placed inside a sealed chamber filled with a inert gas to prevent the oxidation process and control the properties of the material and its qualities [80]. The DED process has several limitations, and advantages over powder bed AM processes like SLM and SLS. Large components (up to several meters) can be easily fabricated using DED, which is currently not possible with the powder bed fusion process. Also, it offers a higher rate of deposition, highly efficient DED system can melt several kg of metal powder per hour [80, 81]. The powder can be changed in the DED process, or mixing is possible during processing to make customised alloy or component with multi-material, which is impossible in SLM and SLS. However, the resolution of the DED process is much lower. Therefore the component fabricated by this process has a poor surface finish which needs major further post-processing, and the manufacturing of more complex geometries, such as overhanging parts, is not possible with DED due to the restriction in the formation of a support structure. Despite the considerable benefits of DED, the research indicates that the most significant application is repairing valuable components [82].

2.7 Electrochemical Additive Manufacturing (ECAM)

Laser-based AM for metals attracts a large audience from different domains of engineering. But conventionally

available AM systems have several limitations, especially when discussing the fabrication of components in micro and nanoscale or even smaller than that. Some reasons behind these limitations are the post-processing of the final component, which is very difficult at the nanoscale, and the inherent size of the metal powder particles used in AM system is generally in the range of 10–100 microns [83]. ECAM combines the electrochemical process and AM to produce structures on a conducting substrate at room temperature from computer-aided design and manufacturing (CAD/CAM) modelling files and addresses the stability challenges that come with it. ECAM offer a substantial benefit over conventional AM processes. Ionic migration is a powerful enough factor to influence the entire deposition process and can also affect the manufactured part's built quality, similar to other issues regarding prior practices. The manufacturing or deposition of amorphous metal at room temperature has several drawbacks, including major residual stress, porosity, limited choice of material, internal stress, anisotropy, strength, stability, etc. It has been shown in numerous investigations that when principles of the traditional electrochemical deposition and AM are integrated, the resulting technique is viable in all key areas [84]. It does not require any thermal processes, lasers, or metal powders, making it more cost-effective and user-friendly. It is produced atomically precise structures with superior quality and stability [85]. The concept of ECAM is the most mathematically and technically logical when compared to other prior AM processes or approaches, as all of the variables that affect the process—such as the voltage, electrolyte, pulse cycle, and interelectrode gap's impact on current density—have a direct mathematical relationship with one another [11, 86, 87]. There are several characteristics of ECAM that can be viewed as advantages over the other existing AM techniques, such as the simplicity of doping, the lack of support structures in ECAM, and the minimization or elimination of

thermal defects in ECAM [11, 86–88]. The most attractive aspect of ECAM is its mask-less nature of work; in all previous deposition versions, the area or pattern to be printed or deposited follows a concept of masking, where the layer of deposition masks or covers a specific area of the electrode [89]. The fabrication method yields noticeably better results, and in all previous iterations of electrodeposition or AM, the printed models have low aspect ratios or small ratios of height to width. Still, if used correctly, the aspect ratio can be adjusted in ECAM to meet specific requirements [90]. It is preferable over other AM alternatives because of the shorter manufacturing time and the considerable reduction in post-processing time [89]. Another intriguing aspect of ECAM is that 3D models can be printed straight from model files thanks to its user-friendly interface (UI) [91]. Using Voxels or volumetric pixels as the foundation of the CAD design that ultimately results in 3D printed prototypes graphically illustrates the amount of automation in ECAM [92].

Due to its ability to manufacture micro-suspensions of metal, ECAM stands out from other AM types [93]. Table 1 highlights the difference between ECAM and other electrodeposition techniques [94]. Expanding the library of readily available materials to produce working devices, meta, or intelligent materials is crucial, which is the practical goal of ECAM. In principle, any material that can be electroplated can also be printed by electrochemical 3D printing, but this requires a precise composition of electrolytes and ink. Copper is used as a printing medium in most existing ECAM-based fabrications. Since copper electrodeposition is simple, easy to manage, and produces fine features. It is known that electrochemical deposition (ECD) is widely used for metals and their different phases, such as binary, ternary, quaternary, metal composites, alloys, multi-materials, conductive polymers, reduced graphene oxide, etc. Likewise, there are some reports available on ECAM printed variety of metals (other than copper), metal alloy, multi-material, and reduced graphene oxide (rGO) micro/nanostructures [95, 96]. According to the printing environment, these techniques can be split into two major groups: (1) Pulsed or direct current (DC) localized electrodeposition (LED) and (2) meniscus-guided electrodeposition (MGED) and are discussed one by one as follows.

2.7.1 Localized Electrodeposition (LED)

Principle In ECAM, the LED works on the same principle as electroplating. Still, in a very accurate and confined way, the movement of metallic ions under the influence of an electric field overcoming the negatively directed double-layer force (if any is present) and deposition on the cathode in a guided way is localized electrodeposition [94]. The control it provides over the process is tremendous, i.e., when the anode move over the surface of the cathode (temporary or permanent substrate), the deposition only occurs at the point of contact. As soon as the anode touches the temporary cathode or substrate, the metallic ions receive the electrons that convert the ions into metal atoms; these metal atoms deposit around the contact area and can be controlled in every way needed [95]. In LED, the surrounding medium where the reaction occurs is liquid, and the anode movement in that conductive medium reduces the metallic ions in its vicinity.

Advantages LED has several advantages over other AM regarding microstructure aspect ratio, its ability to deposit multiple metals, and its compatibility with several types of material. LED avoid all sorts of heating-associated defects, i.e., heat defects, because heat is not used to fuse any atoms; instead, electrical forces are responsible for the deposition [94, 95]. This procedure avoids masking a substrate, making it a mask-less process; masking waste metal and formation in the desired shape beats the purpose of directed AM and rapid prototyping [89]. It supports various materials, making it very cost-effective and low maintenance [94, 95].

Disadvantages The process is not optimum for frequent change in deposition material, as its medium is liquid, i.e., every attempt to change the material in the midst of the deposition process will require the modification of the respective conductive solution; this process is one step process because if paused in between it will lead to inaccuracy and structural errors. If two metallic ions are present in the solution medium, their selective deposition is not possible and neither can the composition be controlled. A nanoscale deposition is complicated in the case of LED because of the surrounding liquid medium since the electrode tip and the contact area cannot reach the nanoscale [90] These are some factors that create a bottleneck situation for the LED process.

Table 1 Common differences between ECAM and other electrodeposition methods

Process	The entire component is made up of the process	After the operation, the cathode is removed	The geometry of a cathode can differ from that of an anode	Deposited area may be localized
Electroplating	No	No	No	No
Electroforming	Yes	Yes	No	No
ECAM	Yes	Yes	Yes	Yes

2.7.1.1 Localized Pulsed Electrodeposition (L-PED) L-PED method enables direct 3D layer-by-layer printing of complicated copper microstructures for various applications, including electronics, metamaterials, plasmonics, and sensors. As mentioned above, conventional DC-ED commonly forms nano- or microcrystalline structures. Metals have reportedly been produced when DC-ED and stirring are combined. DC-ED is a subtype of PED. In L-PED, the deposition is limited to a very narrow zone, which is in between the tip of a nozzle and the desired metal electrolyte periphery zone [86, 91]. The voltage/current between electrodes is periodically turned on and off using a potentiostat, as seen in Fig. 7 a. It employs a large off-time (T_{off}) and a small on-time (T_{on}). As a result, during brief T_{on} periods, a high current density and, as a result, a higher deposition rate can be achieved, whereas during OFF periods, recovery of the consumed ions is happened, and this leads to the placement of a higher ion concentration on cathode surface while there are ON periods [91, 92, 97].

Advantages (1) L-PED significantly increases the limiting current density by supplying ions in the diffusion layer during T_{OFF}. (2) Increased layer density and pore elimination occur in L-PED. (3) Improved layer qualities such as hardness. (4) Galvanic processes are accelerated more rapidly. (5) L-PED can use an additional nozzle or channel to print a support structure if necessary for more complex models.

Disadvantages A few drawbacks exist when ECAM is done in L-PED modes, such as the sole restriction on pattern size in the L-PED method is the travel distance of the printing steps. Also, a pulse rectifier often costs substantially more than a DC unit.

2.7.2 Meniscus-Guided Electrodeposition (MGED)

Principle In ECAM, based on MGED, the principle of working is also the same as of electroplating except for the part where it provides a medium-confined deposition, i.e., unlike the LED, in MGED, the medium is used as a confined controlled path which works as a conductive bridge which connects the anode to the cathode [11, 95]. The conductive liquid is filled in a syringe, which was pre-attached with a micro-nozzle and the liquid containing the metallic ions is allowed to form a meniscus at the tip of the nozzle. The meniscus then is allowed to touch the substrate, and when current is passed via the circuit, metallic ions travel to the surface of the substrate via that meniscus and electrons are transferred to the metallic ions at the substrate's surface. This reaction occurs only in the meniscus vicinity, which can be directed using automated commands, and the freedom of movement is much more significant as the surrounding medium of the meniscus is non-conductive, i.e., air [94, 96, 98].

Advantages The amount of precision offered by MGED is its key advantageous factor. The more control over the process, the more advances and creativity can be employed. The composition of 3D printing is easily tweakable according to researchers' needs [99] and it is easy to form multi-material structures [100]. The concentration of material at the tip of the nozzle can also give us control over the magnetic properties of some materials, for example, Co^{2+} and Cu^{2+}, enabling easy manipulation of the metal composition. The nanoscale deposition is very optimum in the case of MGED, and refined structures at nanoscale are obtained [94, 95].
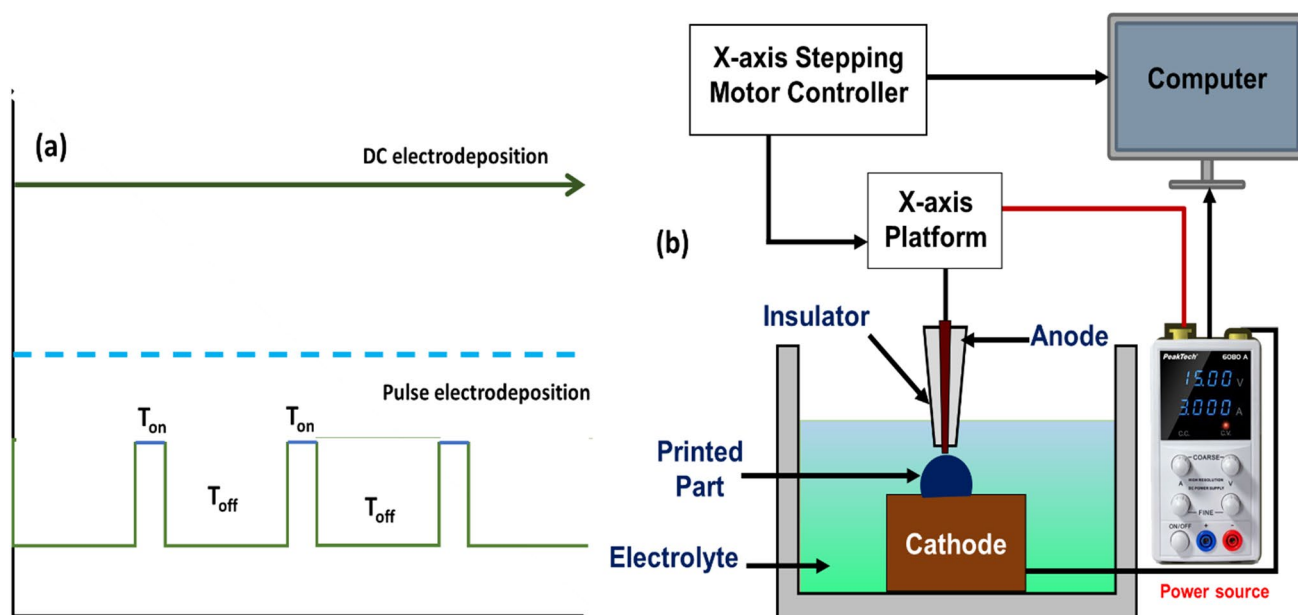

Fig. 7 a Direct current versus pulse current respectively, **b** Schematic representation of Localized electrodeposition AM approach

Disadvantages One of the drawbacks of MGED is its very low compatibility towards rough surfaces; it cannot print conformal structures on rough surfaces without a template, and even in the case of a template, it deforms the structural parameters a bit. Another disadvantage is its time-consuming procedure which fundamentally beats the purpose of rapid prototyping; again, one issue is its limited and selected compatible materials, most of the work is done on metals along with its derivatives and conductive polymers, but the deposition of natural polymers is a far-fetched idea in case of MGED. This process needs a constant supply of ionic motifs, which becomes an issue because even a slight change in ionic concentration can affect the deposition rate[95]. One functional issue reported in the case of nozzle-based models is that their ionic solution sometimes blocks the passage due to the large aggregation of ions at the tip, which is the reason for the constant stirring of solution in experiments with small tips [96].

2.7.3 Design and Methodology

As mentioned above, the ECAM technique has two types, i.e., LED and MGED. An ultra-sharp electrode is submerged in the electrolyte at the conductive substrate, where deposition happens in the LED method, as shown in Fig. 7b. A voltage is then applied between the tip of this ultra-sharp electrode and the conductive substrate to deposit micro and nanostructures on the conductive substrate [89]. Compared to the meniscus-constrained method, LED demonstrates higher deposition rates [89, 91, 94, 95]. Lin et al. [97] observed that voltage and duty cycles have a great significance on the surface morphologies and the micro/nanostructures. Higher voltage and larger duty cycles show more porosity in the structure, and rough surface, whereas lower voltages and low duty cycles result in more dense and finished structures. The main drawback of the LED approach is the inconsistent deposition through localized depletion of species due to a minimal gap between the electrode tip and the substrate [94, 95, 101].

In the MGED approach, as represented in Fig. 8, a print head is filled with electrolyte with a suspended electrode rod inside it act as an anode. With this, a very fine liquid meniscus of electrolyte is established on the tip of the dispensing nozzle in the proximity of the conductive substrate acting as a cathode and the film of metal is deposited on the substrate by reducing metal ions in solution [102, 103]. However, many challenges are there in the way of ECAM as it is still in the infancy stage, and numerous factors are to be researched and studied. The most significant obstacles in the MGED approach are to control the crystallization of metal salt out of solution as a cause of evaporation near the liquid meniscus, which causes blockage at the tip of the pipette because at the low
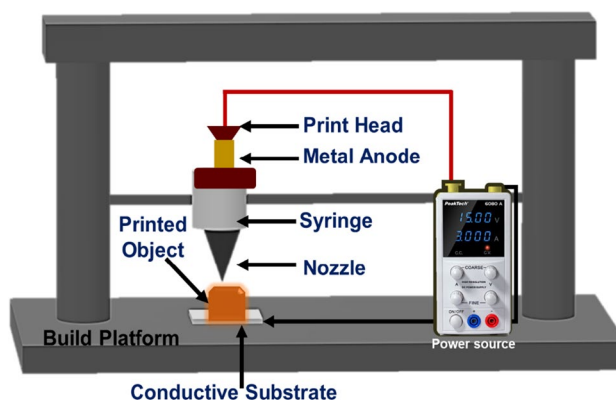

Fig. 8 Schematic representation of MGED ECAM approach

humidity conditions ($< 35\%$) [104]. Metal concentration ions at the meniscus also vary due to evaporation, affecting the deposited structures' morphology and density. Current density is lower for a lower concentration of electrolyte, which slows down the deposition rate but gives smooth surface morphology, whereas higher concentration leads to high current density, in turn, fast deposition rates but gives rough deposition surface morphology [87]. The meniscus stability is essential in the uniform deposition of the material, which depends on the size of the dispensing nozzle and the retraction speed. The meniscus has better stability as the diameter of the dispensing nozzle is decreased, and the evaporation rate is also lowered [105]. Voltage and current are one factor that defines the uniform morphology of the deposited material through electrochemical deposition 3D printing. Suryavanshi and Yu [106] demonstrate 10×10 Cu wire array deposition using a glass pipette aperture of 500 nm. A constant voltage of 0.4 V is applied between the anode and cathode, and retraction speed is 250 nm s^{-1} and the ionic current measured is 2 nA. This experiment demonstrated the uniform deposition of Cu wire of diameter 650 nm of the top cylindrical portion with a base diameter of 950 nm with no porosity and consistent morphology. This study shows that constant voltage and current accordingly play a role in deciding the morphology of the deposited material. Chen et al. [11] deposited dots and lines using $CuSO_4$ with voltages ranging from 1 to 6 V, SEM images were taken for the deposited Cu dots and bars, and it is observed that of all the voltages between 1 and 6 V, 1 V potential gives the most ideal morphology with the dense structure whereas 2 V shows a faster growth rate of dense structure but the deposition is more on the centre thus exhibits convex shape, at 3 V the porosity in the structure increases giving the structure of the dendrite, this is because of the mass transport limitations. At 4 V, Cu deposition becomes dendritic but with fine morphology. This study shows that as go for higher

voltages, the porosity of the structure is increasing, and a non-uniform structure is obtained; however, the deposition rate is increased, but the stability of the meniscus decreases.

2.7.4 Mathematical Model of the System

Various research groups have carried out mathematical modelling and simulation studies of ECAM systems to understand the logic of the process. For example, Kamaraj and Sundaram [91] developed a mathematical model for the deposition rate and layer height of the ECAM system, which showed that the ECAM deposition rate varies from 1 to 3 mm s^{-1} at scan rates of 0.1–2 mm s^{-1}. A tool with a diameter of 250 mm. At large inter-electrode distances, the pulse duty cycle significantly affected the layer height. Ren et al. [107] have investigated the Localized-ECAM technique based on FluidFM to present a mathematical model for pressure-pulse flow in a novel localized fluid transfer process. They also investigated complex, volumetric, linear, and large surface structures in AM.

3 Research Limitations, Implications, and Future Direction

Since the early 2000s, researchers have been working on directly printing 3D nanostructures with controllable microstructures using the ECAM technology [108]. Only a few industrial nations have considered leveraging the links between digitization and manufacturing, theoretically and experimentally. The United States (US), Germany, the United Kingdom (UK), Japan, China, and South Korea [109–112] are some of the emerging players with the highest number of patents related to this technology. These countries have responded instantly and are actively engaged in the deposition at the macro and nanoscale and their characterization. Some of the innovative works are summarized below:

As shown in Fig. 9, the Suryavanshi and Yu [106], reveals that the vertically aligned individual polycrystalline Cu nanowire is deposited via the probe-based electrochemical method, whereas the growth rate is adjusted by applied potential, temperature, and chemical additives. They found that the small diameter of Cu wire can be formed using the nanotube pipette. Similarly, the study of the automated wire-bonding process to the meniscus-confined 3D electrodeposition has been well explored for its essential properties and potential applications in microscale and nanoscale devices [103].

Fig. 9 **a** SEM picture of copper wires with 200 to 250 nm diameters and lengths of 10 μm. **b** SEM image of a copper wire from an isometric perspective **c** copper wire SAED pattern **d** Ionic current versus deposition time graph demonstrating current fluctuation during deposition. And **e** Current versus voltage graph of a 10 μm long copper wire (reproduced with permission from ref. [106]. Copyright 2006, AIP Publishing)
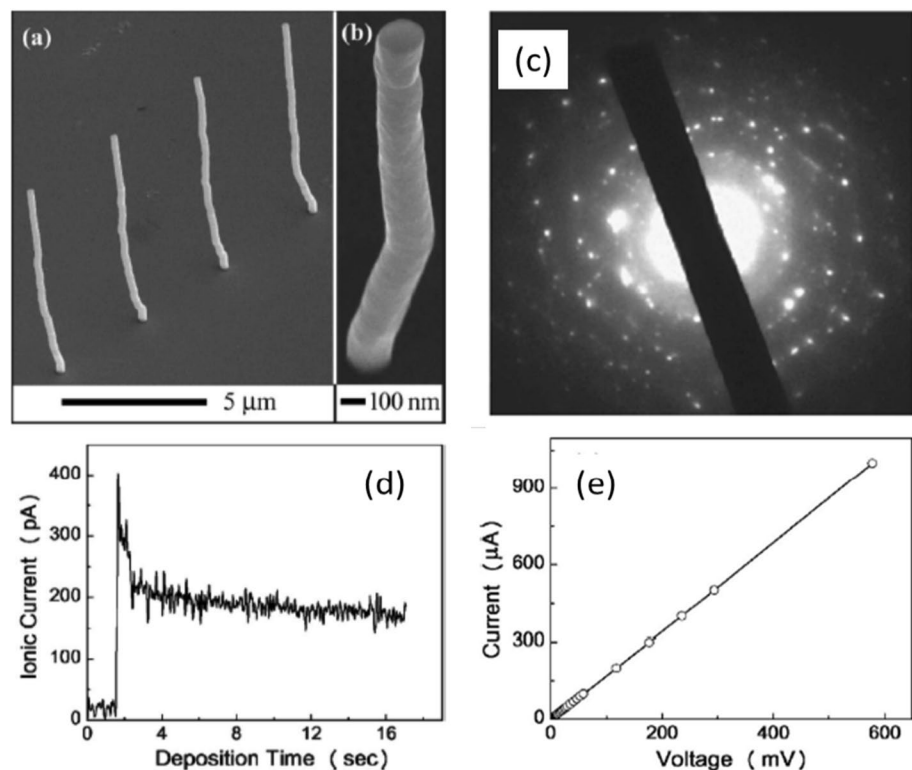
Fig. 10 **a** 20 electrodeposited interconnects with sub-micro-metre widths branching out from a 50 μm by 50 μm central pad. Zoom view of first and second bonds' consistent quality. **b** multilayered connectivity across three 5 μm high stages and **c** overlap interconnects across 5 μm height increments (reproduced with permission from ref. [103]. Copyright 2010, The American Association for the Advancement of Science)
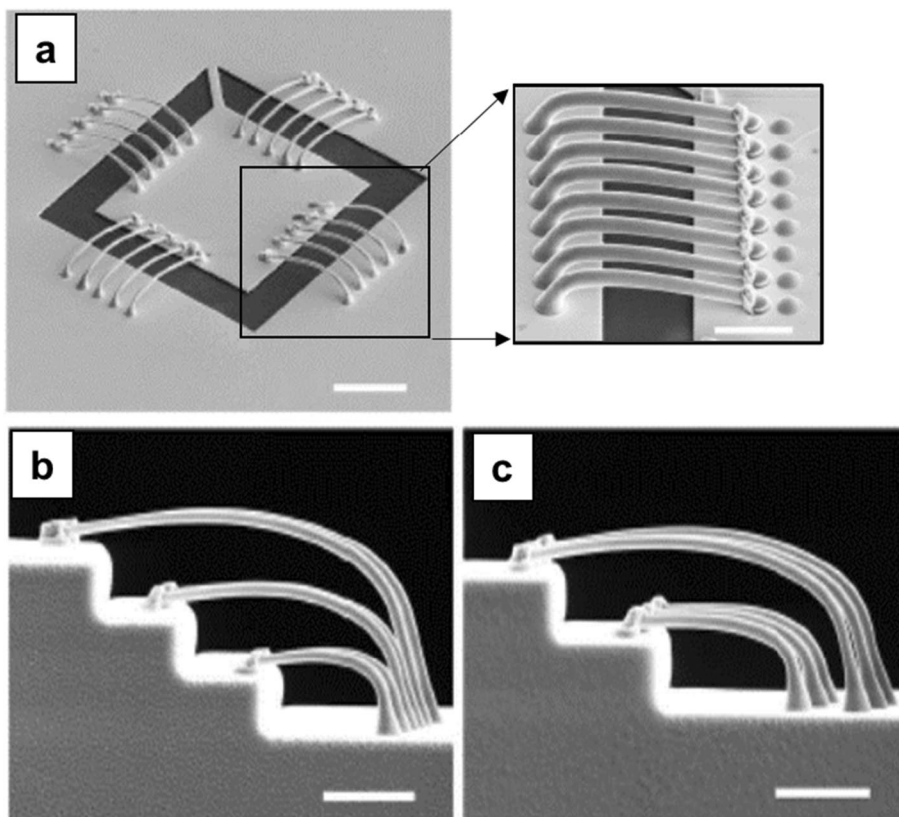
They (Fig. 10) described a connected metal wire grown on the substrate with the nozzle end closed, allowing the electrolyte meniscus below the nozzle to protrude and sub-merge the wire termination and the region of contact on the substrate surface. To accomplish the wire-tie process, they fanned 20 interconnects out from a central bonding pad (Fig. 10b) and also realized that with (Fig. 10b) or with-out (Fig. 10c) multilayered interconnection overlap wiring, the diameter of the Cu wires was found ~ 800 nm with the shaped bonds was ~ 3 mm.

Kim et al. [102] described the manufacturing of nanow-ire-based dense arrays using a simple and versatile electro-deposition approach and analyses of variable fabrication factors like viscosity, evaporation rates, and solvent type. Chen et al. [11] performed optimization of ECAM printer deposition parameters like applied potential and electrolyte concentration and found that they have profound effects on the morphology of deposited copper. A schematic repre-sentation of the physical process of copper ion reduction has been shown in Fig. 11, along with the different deposi-tion potentials ranging from 3 to 6 V. It is observed that the deposition potential increased the resultant surface thickness finish, as highlighted in the micrographs. Kim et al. [113] observed the freestanding rGO nanowires have been grown by an electrochemical 3D printer (Fig. 12); they found a similar function as mentioned above, that the GO meniscus

occurs at the tip of the nozzle, which is reduced via chemi-cal treatment.

The obtained properties confirmed the manufacture of components in electrical devices. In another report, Seol et al. [87] utilized the MGED-ECAM to create freestanding 3D Cu microarchitectures. For the first time, a hollow atomic force microscope (AFM) scanning probes-based single-step approach for 3D metal printing was presented by Hirt et al. [114]. Controlled in-situ growth was visible from the hol-low cantilever's real-time deflection. Morsali et al. [104] investigated the impact of water evaporation from the liquid meniscus at the tip of the nozzle on the deposition of free-standing copper microwires in the MGED-ECAM method. They used multi-physics finite element modelling. Chen et al. [115] described a multi-metal ECAM that was able to create bimetallic geometries with temperature-dependent behaviour, and these printed bimetallic strips have been used in the LED application, as shown in Fig. 13.

They demonstrated that the building up rates are three orders of magnitude higher in compare with the equivalent systems, which is due to the improved mass transport char-acteristics provided by a mechanical electrolyte entrainment mechanism. Their study outlines the ECAM technique's potential and opens the prospect for smarter 3D printed structures. Ambrosi et al. [100] have shown how electro-chemistry may be used to drive multi-material printing
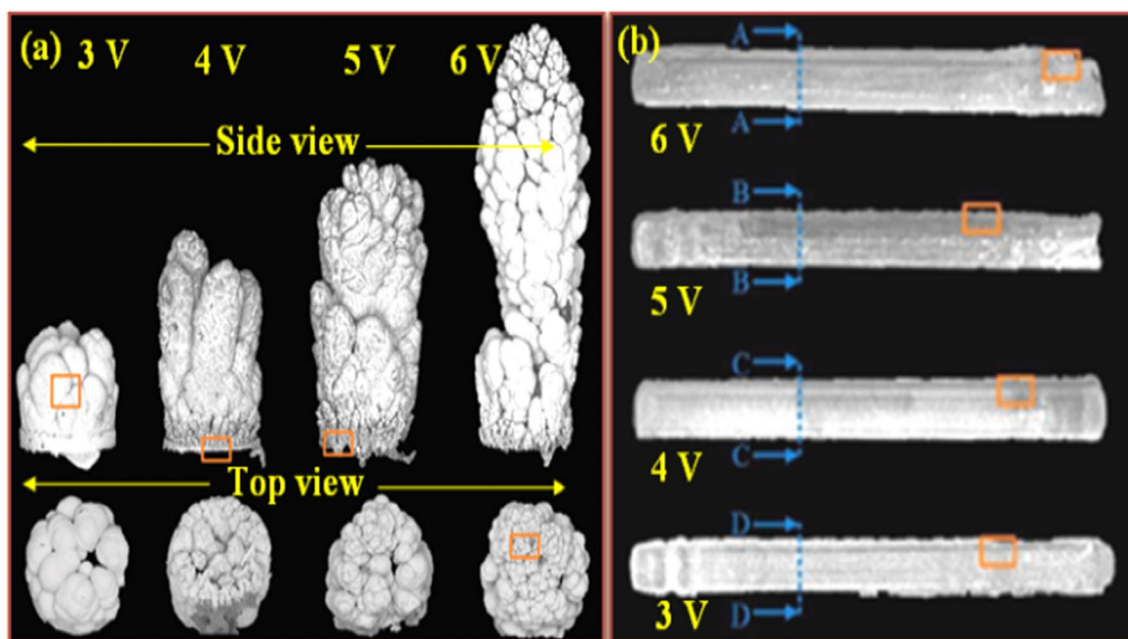
Fig. 11 **a** SEM magnification top and side view, **b** cross-section view of Cu depositions at 3 V to 6 V potentials (reproduced with permission from ref. [11]. Copyright 2017, John Wiley and Sons)

selectively by simply choosing the proper deposition potential. They combined a desktop 3D printer's 3D patterning capability with simultaneous control of the electrochemical process. According to Li et al. [94] ECAM is based on the conventional mask-based electrodeposition process, which has been widely used to fabricate large-scale and precised two-dimensional (2D), and the quasi-three-dimensional (quasi-3D or 2.5D) metallic micro-sized designs and geometries by inversely replicating photoresist through the masks etched lithographically. Several ECAM techniques have been developed to satisfy a wide range of applications, and several have already been commercialized.

Moreover, Siddiqui et al. [116] used an ECAM technique to print a copper electrode for nitrate detection. Large-scale functional structures with complicated geometries cannot be produced by current ECAM systems, e. g. LED and MGED, which require further modifications. However, at a higher deposition rate (19,677 $\mu m^3 s^{-1}$) [11]**,** the ECAM 3D printer can create complex mono- and multi-metal 3D and 4D structures. There are some issues with this nascent technology that must be addressed to improve the system and aid in future research directions:

- All the reported ECAM printers are currently in the prototype stage of proof of concept. To fully automate the system, further work could be done on temperature and voltage control in software, along with an improved meniscus stability control [117].

- The simple mechanical procedure of removing the end product from the substrate can provide a barrier in scaling up and limit component design complexity. Basic research on ECAM has shown that metallic, bimetallic, multi-materials, and graphene structures can be fabricated, opening the door to the fabrication of the sacrificial support structures and facilitate the end product removal the substrate using the well-known chemical removal techniques. However, this still requires further investigation in future works.

- Many electrochemical deposition processes can produce different types of metallic, bimetallic, alloys, multi-materials, graphene, and polymer. Future research could focus on the deposition of those materials by ECAM.

- Meniscus stability is difficult when using the meniscus-controlled method to locate the deposit, as crystal deposits from a residual liquid in the meniscus track would damage the print and result in poor print quality. Other techniques could be explored to increase the durability of localized deposition, such as electrohydrodynamic redox printing, FluidFM electrodeposition, andodified LECD processes [94].

- The moisture management during the ECAM process significantly impacts the growth and deposition rate and geometric and design uniformity of the deposits. Future developments could include precise humidity control systems, which have not yet been considered but have a significant impact.
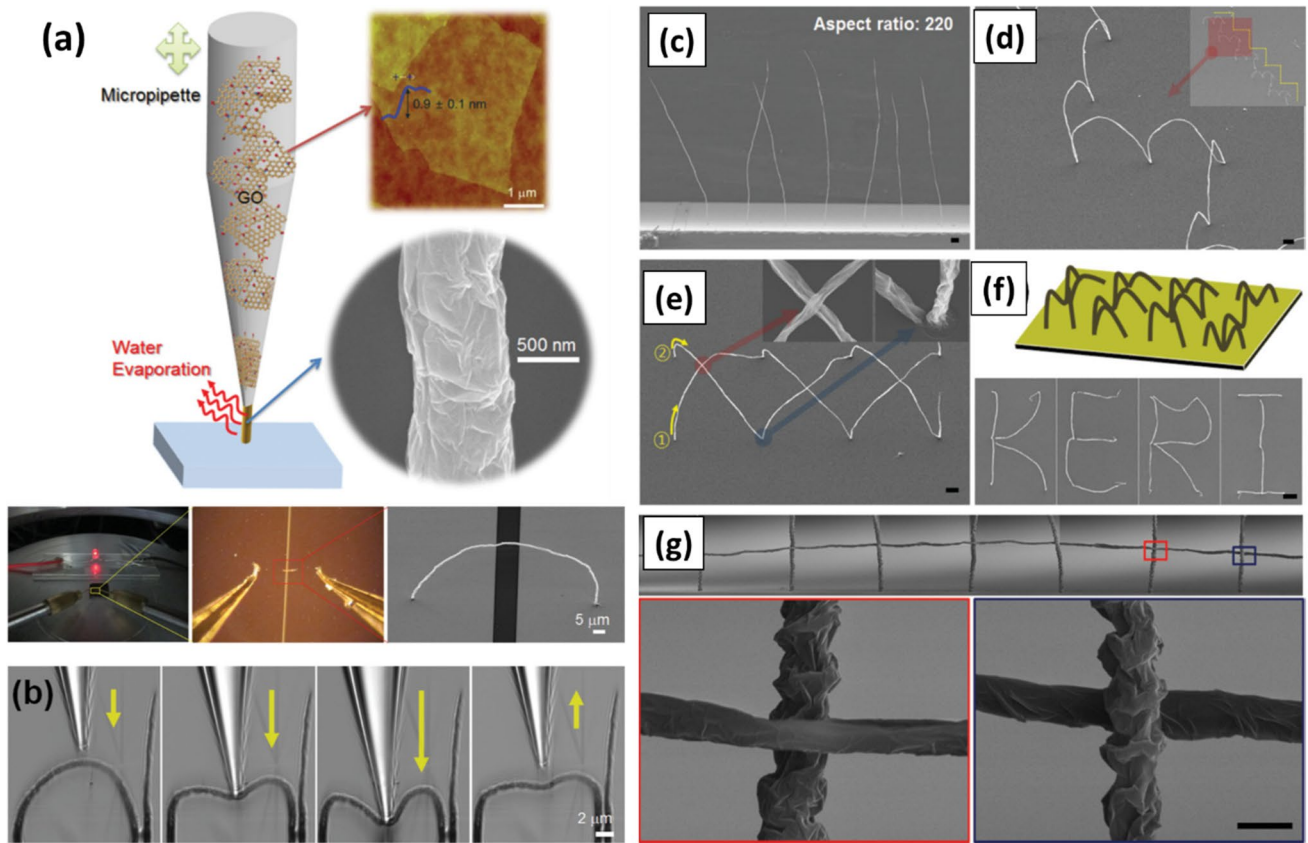
Fig. 12 a Schematic representation of graphene oxide wire manufacturing using an aqueous graphene oxide solution and a micropipette (graphene oxide sheet thickness = 0.9 0.1 nm). Field emission scanning electron microscopic (FE-SEM) picture of rGO wire with r ≈ 400 nm in the circle (bottom right). **b** Optical sequences depicting the bending of the reduced graphene oxide nano-arch. FE-SEM pictures of 3D printing of reduced graphene oxide wire structures with various forms and precise placement are shown in **c–g** (reproduced with permission from ref. [113]. Copyright 2014, John Wiley and Sons)

Fig. 13 A simple electrical circuit activated by the printed bimetallic strip is shown schematically and in pictures (reproduced with permission from ref. [115], under the terms of the Creative Commons CC BY license.)

Table 2 Different AM technologies, including their underlying principles, advantages, issues and other common features

Methods	Principles	Advantages	Issues	Feature resolution (µm)	Typical materials	Ref
BJT	Binder is fed into the raw material powder bed and printed	It is possible to print different colored parts. Ability to print any material, which is available in its powder form. Relatively cheaper	As printed parts are very fragile and have very limited mechanical properties. Unable to fabricate structural parts. Post-prossing in form of casting or sintering are required	25	Intermetallics, polymers, steel, solid oxide fuel cells, $BaTiO_3$, shape memory alloys, magnetic materials, and biodegradable alloys	[13–16]
SLA	Curing of recurring photo-sensitive resins through an UV-laser based energy source	1. Ability to print large objects having surface finish up to 4000 dpi	Low mechanical strengths. Must needed post-curing. Limited number of materials are available	50–100	Ceramics hydrogels, Acrylics, epoxies	[59–62]
Digital light processing (DLP)	Similar to SLA but utilizes light projectors in place of UV lasers	2. No external support is required. 3. High precision objects can be printed		35–120	Polymers, zirconia, composites, elastomers	[8, 9]
SLS	By atomic diffusion, a laser beam is used to sinter the powder particles	Availablity of a wide spectrum of materials. Capability to print complex obects at high deposition rates. Minimal thermal distortion in polymers	Obects are highly porous and have poor surface finish. Operational system is very complex. Very difficult to change the materials	50–100	Nylon,PLA, polymers, metals, metal alloys	[72–78]
SLM	Similar to SLS, here the high power laser beam not just sinter the power particles but metls them till their fusion	High growth rate. Quality products having excellent mechanical properties. Biomedical application metal alloys can be printed	High thermal deformation. Instability of molten pool. Slow in fabrication of complex designs	30–150	Steel, Cp-Ti, cobalt-based alloys, aluminum, ceramics, Ti-6Al- 4 V	[64–67]
ECAM	ECAM produces parts directly from 3D computer models of the parts using the electro-chemical deposition principles with AM	Simple assembly required. Through-mask plating. Localized electrodeposition methods. Post-processing is not required. No requirement of heat treatment	Stability issues. Relatively slow in creating 3D objects	0.050- 10	Metal, metal alloys, bimetallic, conducting polymers, graphene oxide, (Metal nanoparticles fabrication through ECAM process is still in its early stage)	[11, 89, 90, 94, 95, 97, 99–101, 106, 115, 119]

This section provided state-of-the-art information on ECAM, including its fundamental principles, operational models, process characteristics, benefits and drawbacks, obstacles, and future direction. While Comparing the other metal based AM technologies, the ECAM can still produce low-stress geometries, which are free of voids and cracks [86, 101, 118–121]. Because of its excellent potential in the micro- and even nano-metal AM region, ECAM will receive increased attention. Continued research and development in this area are expected to produce a helpful nano-metal AM process.

4 Summary and Outlook

Using a reliable production technique in conjunction with the low-cost manufacturing process for the fabrication abundant materials would be a viable strategy for the industries in future. AM is considered one among the most innovative production technologies to date, and it is gaining widespread interest owing to its ease of use and versatility in producing complicated geometrical components. Unlike conventional manufacturing, such as machining and casting, AM consists of fewer steps and saves material and time in making any functional component. BJT, FDM, SLA, SLS, SLM, and ECAM are the five technologies discussed in Table 2. Apart from the general accessibility of AM methods, there is still space for improvement regarding quality components, processing issues, and 3D-printed items post-treatment. Widespread use of AM in business sectors in several cases. Although the conventional AM techniques had several problems at nano-level fabrication. To overcome this issue, scientific communities are involved in resolving it by introducing electrochemistry into the AM system. However, the substantial quantity of work remains to be entirely understood. Owing to the nature of the atom-by-atom electrochemical deposition process, the ECAM process can be scaled down in size to the nano level. This can be executed both using molecular dynamics simulation and experimental validation. Additionally, the process's scaling-up will be performed to deposit multiple parts simultaneously, either identical to one another or with deliberate differences. Tensile testing will be used to evaluate the output of the Young's modulus, ultimate and yield strengths of the part and to validate a strategic way of achieving isotropy in part using multiple, differently-oriented electrodes.

Declarations

Conflict of interest The authors affirm that they have no known financial or personal conflicts that would have appeared to impact the research presented in this study.

References

1. W.E. Frazier, J. Mater. Eng. Perform. **23**, 1917 (2014)
2. T. Pereira, J.V. Kennedy, J. Potgieter, Procedia Manuf. **30**, 11 (2019)
3. S.H. Huang, P. Liu, A. Mokasdar, L. Hou, Int. J. Adv. Manuf. Technol. **67**, 1191 (2012)
4. A. Mitchell, U. Lafont, M. Hołyńska, C. Semprimoschnig, Addit. Manuf. **24**, 606 (2018)
5. M. Vaezi, H. Seitz, S. Yang, Int. J. Adv. Manuf. Technol. **67**, 1721 (2012)
6. R.B. Kristiawan, F. Imaduddin, D. Ariawan, Z. Arifin, Open Eng. **11**, 639 (2021)
7. C. Xia, Z. Pan, J. Polden, H. Li, Y. Xu, S. Chen, Y. Zhang, J. Manuf. Syst. **57**, 31 (2020)
8. M. Pagac, J. Hajnys, Q.P. Ma, L. Jancar, J. Jansa, P. Stefek, J. Mesicek, Polymers (Basel) **13**, 598 (2021)
9. C.M. González-Henríquez, M.A. Sarabia-Vallejos, J. Rodriguez-Hernandez, Prog. Polym. Sci. **94**, 57 (2019)
10. F. Loffredo, A.D.G. Del Mauro, G. Burrasca, V. La Ferrara, L. Quercia, E. Massera, G. Di Francia, D. Della Sala, Sens. Actuators B Chem. **143**, 421 (2009)
11. X. Chen, X. Liu, P. Childs, N. Brandon, B. Wu, Adv. Mater. Technol. **2**, 1700148 (2017)
12. J.Y. Lee, J. An, C.K. Chua, Appl. Mater. Today **7**, 120 (2017)
13. E. Sachs, M. Cima, P. Williams, D. Brancazio, J. Cornie, J. Eng. Ind. **114**, 481 (1992)
14. N.D. Parab, J.E. Barnes, C. Zhao, R.W. Cunningham, K. Fezzaa, A.D. Rollett, T. Sun, Sci. Rep. **9**, 2499 (2019)
15. M. Ziaee, N.B. Crane, Addit. Manuf. **28**, 781 (2019)
16. X. Lv, F. Ye, L. Cheng, S. Fan, Y. Liu, Ceram. Int. **45**, 12609 (2019)
17. B.P.C. Raghupathy, J.G.P. Binner, J. Am. Ceram. Soc. **94**, 42 (2011)
18. R. Mirzajany, M. Alizadeh, M. Saremi, M.R. Rahimipour, Mater. Lett. **228**, 344 (2018)
19. C.B. Williams, J.K. Cochran, D.W. Rosen, Int. J. Adv. Manuf. Technol. **53**, 231 (2011)
20. J. Suwanprateeb, R. Sanngam, T. Panyathanmaporn, Mater. Sci. Eng. C **30**, 610 (2010)
21. B.R. Utela, D. Storti, R.L. Anderson, M. Ganter, J. Manuf. Sci. Eng. **132**, 0110081 (2010)
22. M. Turker, D. Godlinski, F. Petzoldt, Mater. Charact. **59**, 1728 (2008)
23. K. Lu, M. Hiser, W. Wu, Powder Technol. **192**, 178 (2009)
24. S.I. Yanez-Sanchez, M.D. Lennox, D. Therriault, B.D. Favis, J.R. Tavares, Ind. Eng. Chem. Res. **60**, 15162 (2021)
25. H. Chen, Y.F. Zhao, Rapid Prototyping J. **22**, 527 (2016)
26. C. Schmutzler, T.H. Stiehl, M.F. Zaeh, Rapid Prototyping J. **25**, 721 (2019)
27. H. Miyanaji, N. Momenzadeh, L. Yang, Addit. Manuf. **20**, 1 (2018)
28. E. Mendoza Jimenez, D. Ding, L. Su, A.R. Joshi, A. Singh, B. Reeja-Jayan, J. Beuth, Addit. Manuf. **30**, 100864 (2019)

29. W. Zhang, R. Melcher, N. Travitzky, R.K. Bordia, P. Greil, Adv. Eng. Mater. **11**, 1039 (2009)

30. A. Mostafaei, E.L. Stevens, E.T. Hughes, S.D. Biery, C. Hilla, M. Chmielus, Mater. Des. **108**, 126 (2016)

31. I. Rishmawi, M. Salarian, M. Vlasea, Addit. Manuf. **24**, 508 (2018)

32. A. Yegyan Kumar, Y. Bai, A. Eklund, C.B. Williams, Addit. Manuf. **24**, 115 (2018)

33. K. Sen, T. Mehta, S. Sansare, L. Sharifi, A.W.K. Ma, B. Chaudhuri, Adv. Drug Deliv. Rev. **177**, 113943 (2021)

34. M. Salmi, Materials **14**, 191 (2021)

35. S. Nida, J.A. Moses, C. Anandharamakrishnan, J. Agric. Food Res. **10**, 100392 (2022)

36. P. Shakor, S.H. Chu, A. Puzatova, E. Dini, Prog. Addit. Manuf. **7**, 643 (2022)

37. Y. Yan, Y. Jiang, E.L.L. Ng, Y. Zhang, C. Owh, F. Wang, Q. Song, T. Feng, B. Zhang, P. Li, X.J. Loh, S.Y. Chan, B.Q.Y. Chan, Mater. Today Adv. **17**, 100333 (2023)

38. I. Gibson, D. Rosen, B. Stucker, *Additive Manufacturing Technologies: 3D Printing, Rapid Prototyping, and Direct Digital Manufacturing*, 2nd edn. (Springer, New York, 2015)

39. F. Wulle, D. Coupek, F. Schäffner, A. Verl, F. Oberhofer, T. Maier, Procedia CIRP **60**, 229 (2017)

40. G.W. Melenka, B.K.O. Cheung, J.S. Schofield, M.R. Dawson, J.P. Carey, Compos. Struct. **153**, 866 (2016)

41. A.N. Dickson, J.N. Barry, K.A. McDonnell, D.P. Dowling, Addit. Manuf. **16**, 146 (2017)

42. M. Nabipour, B. Akhoundi, J. Elastomers Plast. **53**, 146 (2020)

43. J. Pratama, S.I. Cahyono, S. Suyitno, M.A. Muflikhun, U.A. Salim, M. Mahardika, B. Arifvianto, Polymers (Basel) **13**, 4022 (2021)

44. B.N. Turner, R. Strong, S.A. Gold, Rapid Prototyping J. **20**, 192 (2014)

45. Q. Sun, G.M. Rizvi, C.T. Bellehumeur, P. Gu, Rapid Prototyping J. **14**, 72 (2008)

46. S. Singh, S. Ramakrishna, R. Singh, J. Manuf. Process. **25**, 185 (2017)

47. C. Bellehumeur, L. Li, Q. Sun, P. Gu, J. Manuf. Process. **6**, 170 (2004)

48. P.K. Penumakala, J. Santo, A. Thomas, Compos. B Eng. **201**, 108336 (2020)

49. J.L. Dávila, M.S. Freitas, P. Inforçatti Neto, Z.C. Silveira, J.V.L. Silva, M.A. DÁvila, J. Appl. Polym. Sci. **133**, 43031 (2016)

50. S. Kumar, J.P. Kruth, Mater. Des. **31**, 850 (2010)

51. F. Castles, D. Isakov, A. Lui, Q. Lei, C.E.J. Dancer, Y. Wang, J.M. Janurudin, S.C. Speller, C.R.M. Grovenor, P.S. Grant, Sci. Rep. **6**, 22714 (2016)

52. T.Z. Sudbury, R. Springfield, V. Kunc, C. Duty, Int. J. Adv. Manuf. Technol. **90**, 1659 (2016)

53. H. Klippstein, A. Diaz De Cerio Sanchez, H. Hassanin, Y. Zweiri, L. Seneviratne, Adv. Eng. Mater. **20**, 1700552 (2018)

54. S. Singh, G. Singh, C. Prakash, S. Ramakrishna, J. Manuf. Process. **55**, 288 (2020)

55. J.W. Choi, F. Medina, C. Kim, D. Espalin, D. Rodriguez, B. Stucker, R. Wicker, J. Mater. Process. Technol. **211**, 424 (2011)

56. C.C. Kuo, Y.R. Wu, M.H. Li, H.W. Wu, Int. J. Adv. Manuf. Technol. **101**, 593 (2018)

57. T.M. Wang, J.T. Xi, Y. Jin, Int. J. Adv. Manuf. Technol. **33**, 1087 (2006)

58. D. Chakraborty, B. AneeshReddy, A. RoyChoudhury, Comput.-Aided Des. **40**, 235 (2008)

59. B. Gross, S.Y. Lockwood, D.M. Spence, Anal. Chem. **89**, 57 (2017)

60. D.H. Ko, K.W. Gyak, D.P. Kim, J. Flow Chem. **7**, 72 (2017)

61. S. Wu, J. Serbin, M. Gu, J. Photochem. Photobiol. A Chem. **181**, 1 (2006)

62. M. Rodas Ceballos, F. González Serra, J.M. Estela, V. Cerdà, L. Ferrer, Talanta **196**, 510 (2019)

63. A. Bove, F. Calignano, M. Galati, L. Iuliano, Appl. Sci. **12**, 3591 (2022)

64. C.Y. Yap, C.K. Chua, Z.L. Dong, Z.H. Liu, D.Q. Zhang, L.E. Loh, S.L. Sing, Appl. Phys. Rev. **2**, 041101 (2015)

65. C.C. Ng, M.M. Savalani, H.C. Man, I. Gibson, Virtual Phys. Prototyp. **5**, 13 (2010)

66. N.T. Aboulkhair, M. Simonelli, L. Parry, I. Ashcroft, C. Tuck, R. Hague, Prog. Mater. Sci. **106**, 100578 (2019)

67. E.O. Olakanmi, R.F. Cochrane, K.W. Dalgarno, Prog. Mater. Sci. **74**, 401 (2015)

68. E. Brandl, U. Heckenberger, V. Holzinger, D. Buchbinder, Mater. Des. **34**, 159 (2012)

69. E.M. Sefene, J. Manuf. Syst. **63**, 250 (2022)

70. F. Murat, I. Kaymaz, A.T. Şensoy, I.H. Korkmaz, Met. Mater. Int. **29**, 59 (2023)

71. M.E. Korkmaz, M.K. Gupta, G. Robak, K. Moj, G.M. Krolczyk, M. Kuntoğlu, J. Manuf. Process. **81**, 1040 (2022)

72. E.O. Olakanmi, Mater. Res. **15**, 167 (2012)

73. A. Mokrane, M. Boutaous, S. Xin, Comptes Rendus Mécanique **346**, 1087 (2018)

74. A. Mazzoli, Med. Biol. Eng. Comput. **51**, 245 (2012)

75. F. Fina, A. Goyanes, C.M. Madla, A. Awad, S.J. Trenfield, J.M. Kuek, P. Patel, S. Gaisford, A.W. Basit, Int. J. Pharm. **547**, 44 (2018)

76. D. Drummer, D. Rietzel, F. Kühnlein, Phys. Procedia **5**, 533 (2010)

77. S. Fish, J.C. Booth, S.T. Kubiak, W.W. Wroe, A.D. Bryant, D.R. Moser, J.J. Beaman, Addit. Manuf. **5**, 60 (2015)

78. A.N. Chen, M. Li, J.M. Wu, L.J. Cheng, R.Z. Liu, Y.S. Shi, C.H. Li, J. Alloys Compd. **776**, 486 (2019)

79. W. Han, L. Kong, M. Xu, Int. J. Extreme Manuf. **4**, 042002 (2022)

80. D. Svetlizky, B. Zheng, A. Vyatskikh, M. Das, S. Bose, A. Bandyopadhyay, J.M. Schoenung, E.J. Lavernia, N. Eliaz, Mater. Sci. Eng. A **840**, 142967 (2022)

81. Z. Sun, W. Guo, L. Li, Addit. Manuf. **33**, 101175 (2020)

82. G. Piscopo, L. Iuliano, Int. J. Adv. Manuf. Technol. **119**, 6893 (2022)

83. S. Shailendar, M.M. Sundaram, Mater. Manuf. Process. **31**, 81 (2015)

84. M. Sundaram, A.B. Kamaraj, G. Lillie, Procedia CIRP **68**, 227 (2018)

85. S.A. Hassankiadeh, A. Sadeghi, J. Appl. Phys. **123**, 214501 (2018)

86. A.B. Kamaraj, M. Sundaram, Int. J. Adv. Manuf. Technol. **102**, 2367 (2019)

87. S.K. Seol, D. Kim, S. Lee, J.H. Kim, W.S. Chang, J.T. Kim, Small **11**, 3896 (2015)

88. R. Sreenivasan, A. Goel, D.L. Bourell, Phys. Procedia **5**, 81 (2010)

89. M.M. Sundaram, A.B. Kamaraj, V.S. Kumar, J. Manuf. Sci. Eng. **137**, 021006 (2015)

90. J.D. Madden, I.W. Hunter, J. Microelectromech. Syst. **5**, 24 (1996)

91. A.B. Kamaraj, M. Sundaram, J. Appl. Electrochem. **48**, 463 (2018)

92. A.B. Kamaraj, H. Shrestha, E. Speck, M. Sundaram, Procedia Manuf. **10**, 478 (2017)

93. S.M.H. Hashemi, U. Babic, P. Hadikhani, D. Psaltis, Curr. Opin. Electrochem. **20**, 54 (2020)

94. X. Li, P. Ming, S. Ao, W. Wang, Int. J. Mach. Tools Manuf. **173**, 103848 (2022)

95. J. Hengsteler, G.P.S. Lau, T. Zambelli, D. Momotenko, Electrochem. Sci. Adv. **2**, e2100123 (2022)

96. V. Chauhan, N. Singh, M. Goswami, S. Kumar, M.S. Santosh, N. Sathish, P. Rajput, A. Mandal, M. Kumar, P.N. Rao, M. Gupta, S. Kumar, Appl. Phys. A **128**, 458 (2022)

97. J.C. Lin, T.K. Chang, J.H. Yang, Y.S. Chen, C.L. Chuang, Electrochim. Acta **55**, 1888 (2010)

98. N. Singh, H. Siddiqui, S. Kumar, M. Goswami, A. Kumar, T. Sharda, S. Kumar, N. Sathish, A.K. Srivastava, Mater. Lett. **307**, 130976 (2022)

99. J. Hengsteler, B. Mandal, C. van Nisselroy, G.P.S. Lau, T. Schlotter, T. Zambelli, D. Momotenko, Nano Lett. **21**, 9093 (2021)

100. A. Ambrosi, R.D. Webster, M. Pumera, Appl. Mater. Today **18**, 100530 (2020)

101. J. Xu, W. Ren, Z. Lian, P. Yu, H. Yu, Int. J. Adv. Manuf. Technol. **110**, 1731 (2020)

102. J.T. Kim, S.K. Seol, J. Pyo, J.S. Lee, J.H. Je, G. Margaritondo, Adv. Mater. **23**, 1968 (2011)

103. J. Hu, M.F. Yu, Science **329**, 313 (2010)

104. S. Morsali, S. Daryadel, Z. Zhou, A. Behroozfar, D. Qian, M. Minary-Jolandan, J. Appl. Phys. **121**, 024903 (2017)

105. S. Morsali, S. Daryadel, Z. Zhou, A. Behroozfar, M. Baniasadi, S. Moreno, D. Qian, M. Minary-Jolandan, J. Appl. Phys. **121**, 214305 (2017)

106. A.P. Suryavanshi, M.F. Yu, Appl. Phys. Lett. **88**, 083103 (2006)

107. W. Ren, J. Xu, Z. Lian, P. Yu, H. Yu, Materials **13**, 2783 (2020)

108. R.A. Said, Nanotechnology **15**, S649 (2004)

109. D.M. Wirth, D.F. Pain, J.W. Herman, United States Patent, US9777385B2 (2017)

110. Q. Huang, United States Patent, US11008664B2 (2021)

111. M.M. Sundaram, United States Patent, US10501857B2 (2019)

112. D.T. Schwartz, J.D. Whitaker, United States Patent, US7615141B2 (2009)

113. J.H. Kim, W.S. Chang, D. Kim, J.R. Yang, J.T. Han, G.W. Lee, J.T. Kim, S.K. Seol, Adv. Mater. **27**, 157 (2015)

114. L. Hirt, S. Ihle, Z. Pan, L. Dorwling-Carter, A. Reiser, J.M. Wheeler, R. Spolenak, J. Vörös, T. Zambelli, Adv. Mater. **28**, 2311 (2016)

115. X. Chen, X. Liu, M. Ouyang, J. Chen, O. Taiwo, Y. Xia, P.R.N. Childs, N.P. Brandon, B. Wu, Sci. Rep. **9**, 3973 (2019)

116. H. Siddiqui, N. Singh, V. Chauhan, N. Sathish, S. Kumar, Mater. Lett. **305**, 130795 (2021)

117. H. Siddiqui, N. Singh, D. Katiyar, P. Naidu, S. Mishra, H. Chandra Prasad, M. Akram Khan, M. Ashiq, N. Sathish, S. Kumar, Mater. Today Proc. **72**, 2741 (2023)

118. T.M. Braun, D.T. Schwartz, Electrochem. Soc. Interface **25**, 69 (2016)

119. Y.T. Tseng, J.C. Lin, J. Shian-Ching Jang, P.H. Tsai, Y.J. Ciou, Y.R. Hwang, ACS Appl. Electron. Mater. **2**, 3538 (2020)

120. M. Sundaram, A. Drexelius, A.B. Kamaraj, Mach. Sci. Technol. **23**, 232 (2018)

121. F. Zhang, Z. Yao, O. Moliar, Z. Zhang, X. Tao, Surf. Coat. Technol. **403**, 126404 (2020)